Implementation of polarization processes in a charge transport model applied on poly(ethylene naphthalate) films

M.-Q. Hoang, Séverine Le Roy, Laurent Boudou, G. Teyssedre

Implementation of Polarization Processes in a Charge Transport Model applied on Poly(ethylene naphthalate) Films

M-Q. Hoang, S. Le Roy, L. Boudou, G. Teyssedre

LAPLACE, Université de Toulouse, CNRS, INPT, UPS, France

To cite: M-Q. Hoang, S. Le Roy, L. Boudou, G. Teyssedre, "*Implementation of polarization processes in a charge transport model applied on Poly(ethylene naphthalate) films*", J. Appl. Phys. 119, 224105, 2016. DOI: 10.1063/1.4953646

Abstract—**One of the difficulties in unravelling transport processes in electrically insulating materials is the fact that the response, notably charging current transients, can have mixed contributions, from orientation polarization and from space charge processes. This work aims at identifying and characterizing the polarization processes in a polar polymer in the time and frequency-domains, and to implement the contribution of the polarization into a charge transport model. To do so, Alternate Polarization Current (APC) and Dielectric Spectroscopy (DS) measurements have been performed on poly(ethylene naphthalene 2,6-dicarboxylate) (PEN), an aromatic polar polymer, providing information on polarization mechanisms in the time-domain and frequency-domain respectively. In the frequency-domain, PEN exhibits 3 relaxation processes termed β, β* (sub-glass transitions) and α relaxations (glass transition) in increasing order of temperature. Conduction was also detected at high temperatures. Dielectric responses were treated using a simplified version of the Havriliak-Negami (HN) model (Cole-Cole (CC) model), using 3 parameters per relaxation process, these parameters being temperature dependent. The time dependent polarization obtained from the CC model is then added to a charge transport model. Simulated currents issued from the transport model implemented with the polarization are compared to the measured APC currents, showing a good consistency between experiments and simulations in a situation where the response comes essentially from dipolar processes.**

I. INTRODUCTION

Charge transport models, or fluid models, have been increasingly developed this last decade[1-4] for solid organic dielectrics, and are mainly applied to polyethylene-based materials. These models could be of great help to predict the space charge and field distributions under any electrical stress, and are indeed useful to build and refine ageing and life models for insulating materials. These models, generally one dimensional and bipolar, take into account electronic charges generation and transport in the material, and some specific processes such as trapping and recombination. Although good correlation between experimental and simulation results has been reached for low density polyethylene (LDPE)[1,3], these models remain unable to describe the dielectric response short time after application of the voltage[5], and are far from describing the material behavior under thermo-electrical stress[6]. This lack of correlation is mainly due to the fact that other processes not linked to transport also take place, and are not included in these models. This is particularly the case for polar polymers, as polarization processes can provide noticeable response in the time scale of interest – i.e. seconds to minutes-, depending on actual temperature and on the occurrence of relaxation processes. Our aim is to make these fluid models evolve to take into account polar mechanisms. However, one of the difficulties in unravelling transport processes from other processes is the fact that the response, notably charging current transients, can have mixed contributions from orientation polarization and from space charge processes. To account for polarization phenomena in the model, the variation of the material permittivity (ε) as a function of temperature and frequency or time must be known. The permittivity depends on the experimental conditions (mainly temperature and polarization time). Its characterization can be done in the time-domain (by means of Isothermal charging/discharging currents, Thermo-Stimulated Depolarization Current measurements –TSDC as examples) and in the frequency-domain (Impedance Spectroscopy measurements). Whatever the characterization domain, time or frequency, the experimental data treatment remains difficult[7] to obtain the material relaxation function. Although dielectric spectroscopy has been performed with some success on LDPE, a non-polar material[8], it remains also difficult to obtain a complete characterization of its permittivity dependence as a function of temperature and frequency. Hence, Poly(ethylene naphthalene 2,6-dicarboxylate) (PEN)

has been chosen for this study as it is an aromatic polar polymer, and is known to give a significant dipolar response[9,10] for different measurement techniques. In what follows, we address only the validation of the fluid model in terms of polarization, as a huge work of parameterization should be done for charge transport processes in PEN (trapping, detrapping parameters, injection barrier height…), requiring a large amount of experimental results. The polarization will be considered as a linear process with field, since except for ferroelectric materials, a non-linear response such as polarization saturation, is not reached before breakdown.

In our work, dielectric spectroscopy (DS) measurements, a well-known technique for performing a complete characterization of the dielectric relaxations, were carried out in order to characterize the dipolar response of the material in the frequency-domain. This response is then fitted to Havriliak-Negami functions, converted in the time domain, and introduced into a fluid model already developed[1]. The model results are validated at different temperatures by current measurements under low fields using the Alternate Polarization Current -APC- method[11]. A discussion on the model validation is proposed in the last part of this paper.

II. DS MEASUREMENTS AND DATA PROCESSING

A. Samples and Measurement Conditions

Semi-crystalline PEN films are commercial TEONEX® Q51 films provided by DuPont Teijin Films Co. The melting temperature is ~~of~~ 269°C and the glass transition temperature is 121°C[12]. Test films of 188 µm thickness were coated on each face with 16 mm-diameter circular gold electrodes. DS measurements were carried out using a Novocontrol Alpha-A analyzer over a frequency range from 10^{-1} to 10^{6} Hz, and over a temperature range from -100 to 200°C by step of 5°C. The films crystallinity, determined by Differential Scanning Calorimetry, is 41%. This value does not change when the sample is subjected to an annealing treatment at temperatures up to at least 170°C[9].

B. Experimental Results

DS results are presented in Figure 1 as a function of log(frequency) for different temperatures. The dielectric constant, ε' (Figure 1a), weakly decreases over the frequency range, while it increases with the temperature. Figure 1b shows the imaginary part of the permittivity, i.e. dielectric losses ε". Three relaxation peaks are observed, labelled β, β*, and α, in increasing order of temperature. The first one, called β, is observed at low temperatures, and is assigned to local fluctuations of ester groups (O-C=O) similar to the β-process in Poly(ethylene terephthalate) (PET)[13,14]. The β-peak shifts towards higher frequencies when the temperature increases.

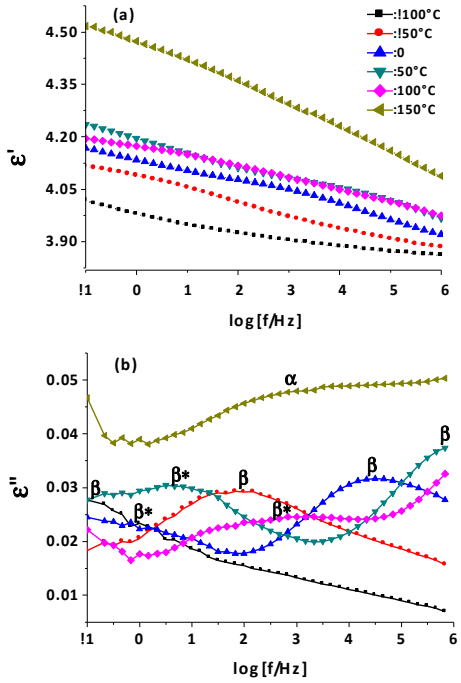

FIG. 1. Dielectric constant (a) and loss (b) vs. log(frequency) for PEN as a function of temperature

Although only one peak is observed for the β-process at low temperatures, Bravard et al.[7], in the study of PEN, PET and their copolymers, indicated that this β-process, being asymmetric, would be better represented as a composite of two overlapping symmetric processes, β_1 and β_2. Hakme et al.[15] have shown that, on amorphous PEN, the β_2-process amplitude strongly depends on humidity content in the samples; the β_1-process amplitude depends on the drawing ratio and the stretched temperature.

The second peak, called β^*, is observed for temperatures in the range of -50°C up to 100°C. This β*-peak also shifts towards higher frequencies when the temperature increases. In the literature, it has been attributed to the relative motion of the two naphthalene rings present in the polymer chain[16]. The mechanisms associated with this relaxation process are dependent upon ~~the~~ measurement frequency[17], and are still a matter of debate. As an example, this peak was not observed in the case of PET. This result could be linked to the presence of a naphthalene ring in PEN, whereas PET only has one phenyl ring. However, Illers et al.[18], investigating the mechanical secondary β relaxation of PET on the basis of isochronal temperature scans of torsion modulus and damping, have suggested the presence of three peaks β_1, β_2 and β_3 at low temperatures. This suggestion was also proposed by Bravard et al.[7]. The third (β_3) process, probably equivalent to the β^*-process of PEN, is thought to be due to the presence of COO-groups adjacent to phenyl rings in different configurations.

The third peak, called α, observed at high temperatures, is clearly related to the glass transition of PEN, involving long-range cooperative segments motion[19]. The α-relaxation is naturally originating from

a conformational collective rearrangement of the chains in the material amorphous regions. The α-relaxation peak amplitude decreases as a result of crystallization[20]. Conduction was also detected at temperatures above the α-peak (150°C) in the low frequency range.

However, these three relaxations never appear simultaneously in the experimental frequency windows (10^{-1} to 10^{6} Hz) when working in isothermal conditions. It is also difficult to separate one relaxation when working with a temperature ramp for a fixed frequency. It is then necessary to model the global dielectric response of PEN, working on different temperature ranges for each relaxation.

C. Data Processing

An empirical model of Havriliak and Negami[21] is used to describe the dielectric relaxations. The variation of the complex permittivity $\varepsilon^*(\omega)= \varepsilon'(\omega)-j\ \varepsilon''(\omega)$ is given by:

$$\varepsilon^*(\omega) = \varepsilon_\infty + \frac{\Delta\varepsilon}{\left[1+(j\omega\tau)^b\right]^c} \qquad (1)$$

where $\omega=2\pi f$ is the electric field pulsation, $\Delta\varepsilon=\varepsilon_s-\varepsilon_\infty$ is the dielectric dispersion of the relaxation, ε_s and ε_∞ are the relaxed ($\omega=0$) and unrelaxed ($\omega=\infty$) dielectric constant ~~values~~, τ is the relaxation time associated with the relaxation, b and c ($0\leq b, c\leq 1$) are shape parameters which describe the symmetric and the asymmetric broadening of the relaxation time distribution function, respectively. In the PEN dielectric loss spectra, relaxation peaks are relatively symmetric. For this reason, we used the Cole-Cole function[22], a particular case of the Havriliak-Negami function with c=1, to model the dielectric response. Taking into consideration the different relaxation modes and adding a conduction term to ε^*, a complete relaxation function is obtained:

$$\varepsilon^*(\omega) = \varepsilon_\infty + \sum_{i=1}^{n} \frac{\Delta\varepsilon_i}{1+(j\omega\tau_i)^b} + \frac{\kappa}{\varepsilon_0 (j\omega)^s} \qquad (2)$$

where $\varepsilon_0=8.85.10^{-12}$ F.m^{-1} is the permittivity of vacuum, κ is a conduction term and s is a parameter related to the nature of the conduction mechanism ($0\leq s\leq 1$). For PEN, 3 relaxations are observed (n=3), so there are 12 parameters that need to be fitted, all of them being potentially temperature dependent.

In order to fit the entire dielectric loss response of the semi-crystalline PEN, we used an extrapolation method that was first proposed by Coburn et al.[14] for studying the PET relaxations, and widely applied to PEN[7,23]. The fit by a Cole-Cole function was done for all ~~the~~ temperatures where the maximum of dielectric loss was well defined in the experimental frequency window.

The dielectric losses vs. frequency in the β-relaxation temperature region (from -80°C to -20°C) are presented in Figure 2. As discussed above, the β-process has been described in the literature as the sum of two overlapping symmetric processes, β_1 and β_2.

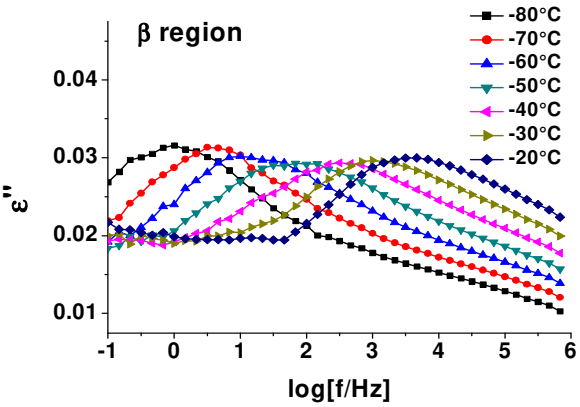

FIG. 2. Dielectric loss vs. log(frequency) in the β-relaxation region of PEN.

Figure 3 shows the fit of dielectric loss at -80°C by a sum of two Cole-Cole functions. When the β_1 and β_2 modes in the explored frequency-window can be appropriately distinguished, as is the case here, reliable parameters can be achieved. However, this is no longer the case when rising the temperature since the two modes overlap. Therefore, for sake of simplification we fitted the β relaxation as a unique contribution. This has no real impact on the predicted results in time domain as the characteristic times are longer.

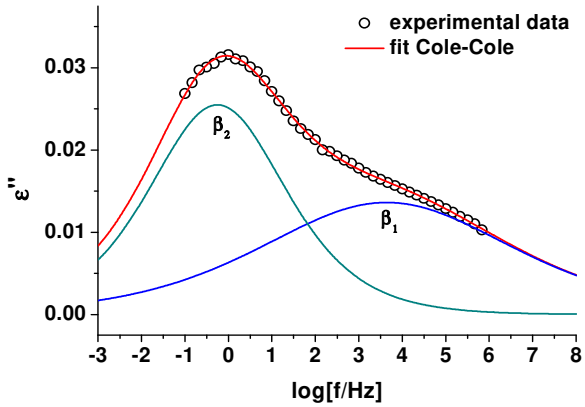

FIG. 3. Fit of the β-relaxation of PEN at -80°C to two Cole-Cole components.

For this β relaxation, a set of Cole-Cole parameters able to fit the dielectric loss and permittivity vs. frequency was obtained. An example of comparison between the fit (solid line) and the experimental dielectric losses (symbols) vs. frequency at -50°C is given in Figure 4a. The fit was performed around the peak maximum (between the two vertical dashed lines on Figure 4a in order to avoid the possible contributions from other relaxations). The parameters variation with temperature, presented in Figure 5 (open triangles), are described by equations (3)-(5):

$$\Delta\varepsilon_\beta = 0.263 - 7.796.10^{-10}T \qquad (3)$$

$$b_\beta = -0.065 + 1.452.10^{-3}T \qquad (4)$$

$$\ln \tau_\beta = -39.307 + \frac{0.634}{k_B T} \text{ with } \tau_\beta \text{ in s} \qquad (5)$$

where T is the temperature, in Kelvin, and k_B=8.617.10^{-5} eV.K^{-1} is Boltzmann's constant. Δε and b follow nearly a linear variation with temperature, while ln τ decreases linearly with the reciprocal of the absolute temperature, following the Arrhenius law. The activation energy value for this β relaxation (0.634 eV or 61 kJ/mol) is in the range of what is reported in the literature for PEN using dielectric spectroscopy[24], i.e. between 51 and 69 kJ/mol, depending on the crystallinity of the samples.

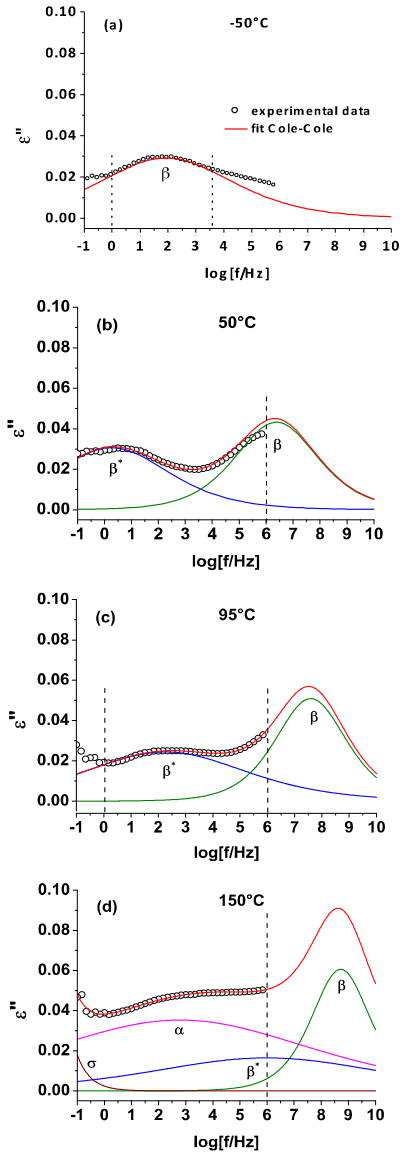

FIG. 4. Dielectric loss for PEN as a function of temperature. Experimental data and fit results at: a) -50°C; b) +50°C; c) 95°C; d) 150°C.

For the β*-relaxation peak, the best approximations were found for temperatures ranging from 85 to 110°C where the dielectric loss maximum was well defined in the experimental frequency window. The parameters found for this peak are, however, valid over the range of temperatures from 30 to 110°C, where the peak appears, even partially, in the frequency window.

To fit the β* peak, it is necessary to take into account the overlapping β-process at high frequencies. This was done by adding to the β*-peak contribution the extrapolation of the β-peak contribution using equations (3)-(5) in the β*-peak temperature region (filled triangles in Figure 5). The experimental values of ε" in this region were fitted using the equation:

$$\varepsilon''(\omega) = \varepsilon''_\beta(\omega) + \varepsilon''_{\beta^*}(\omega) \qquad (6)$$

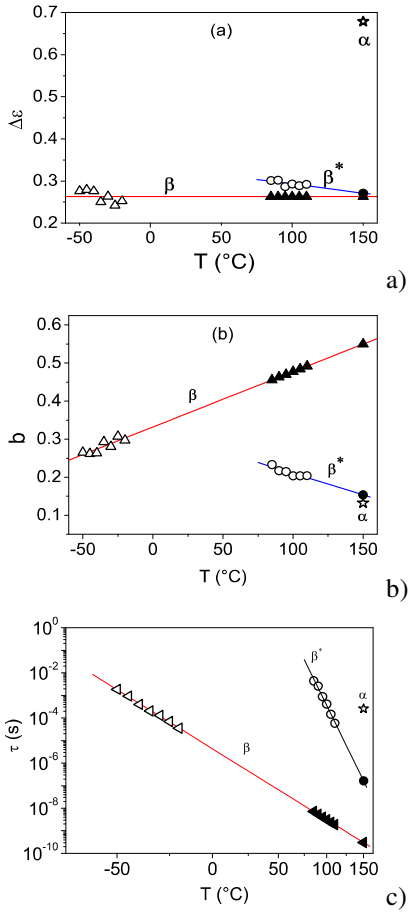

FIG. 5. Cole-Cole parameters vs. temperature obtained from fit method and used as extrapolated data. Open symbols correspond to fitting parameters; filled symbols correspond to extrapolated parameters. β-relaxation: triangles; β*-relaxation: circles. (a) relaxation strength Δε; (b) Cole-Cole exponent b; (c) relaxation time in an Arrhenius diagram.

Figures 4c shows the comparison between the experimental result and the fit for the β* contribution at 95°C performed in the frequency region from 1 to 10^6 Hz, where the contribution from α-process can be neglected. By doing so for all the temperatures ranging from 85 to 110°C, a set of Cole-Cole parameters for the β*-peak was obtained. This set is presented in Figure 5 (open circles), and fitted by equations (7)-(9):

$$\Delta\varepsilon_{\beta^*} = 0.456 - 4.352.10^{-4} T \qquad (7)$$

$$b_{\beta^*} = 0.631 - 1.129.10^{-3} T \qquad (8)$$

$$\ln \tau_{\beta^*} = -72.958 + \frac{2.090}{k_B T} \quad (9)$$

For the β* relaxation, the activation energy (2.09 eV = 201.7 kJ/mol) is higher compared to what has been found in the literature using dielectric spectroscopy (maximal value= 111 kJ/mol). It is however in the activation energies range measured using Dynamic Mechanical Analysis (DMA) for PEN samples of different crystallinity, i.e. between 119 and 247 kJ/mol[24].

Finally, the same procedure was used to obtain parameters related to the α-relaxation and the conduction σ. In this case we used the equation:

$$\varepsilon''(\omega) = \varepsilon''_{\beta}(\omega) + \varepsilon''_{\beta^*}(\omega) + \varepsilon''_{\alpha}(\omega) + \sigma''(\omega) \quad (10)$$

The extrapolation of the β and β* contributions was done using equations (3)-(5) and (7)-(9) respectively in the α-peak temperature region (filled triangles and filled circles in Figure 5). Figure 4d shows the dielectric loss fit at 150°C in the full experimental frequency range with all contributions (β, β*, α and conduction). The set of Cole-Cole parameters for the α-process at 150°C is as follows:

$\Delta_{\varepsilon\alpha}$=0.679; b_α=0.132; τ_α=2.61 10^{-4}s.

Analysis of the temperature dependence of the parameters for this α-process was not achieved owing to the superposition with conduction phenomena and limited temperature variation of the relaxation.

III. IMPLEMENTATION OF THE POLARIZATION IN THE FLUID MODEL

A. Evolution of the fluid model equations

The fluid model has already been presented in the literature[1] for polyethylene. It predicts measurable macroscopic parameters such as external current, which is of interest in the present study.

The model is based on Poisson's, transport and continuity equations. Until now, the permittivity was considered in this model as a constant, regardless of the experimental conditions. In order to implement the variation of the permittivity in the charge transport model, the Poisson's equation and the external current equation need to be rewritten as Maxwell-Gauss and Maxwell-Ampere equations, respectively:

$$\nabla D(x,t) = \rho(x,t) \quad (11)$$

$$J(x,t) = j_c(x,t) + \frac{\partial D(x,t)}{\partial t} \quad (12)$$

where ρ(x,t) is the net charge density, function of time and space, and j_c(x,t) is the local conduction current. D(x,t) is the electrical displacement, which encompasses the polarization processes. Hence, if there is no conduction (i.e. the first term j_c(x,t) is null), or if the conduction processes are not dominant, the external current density J(x,t) is due to polarization variation.

B. Calculation of the electrical displacement

The electrical displacement D(x,t) is given in the frequency domain by[25]:

$$D(\omega) = \varepsilon_0 \varepsilon^*(\omega) E(\omega) \quad (13)$$

where E is the electric field and ε*(ω) the material relative permittivity defined by the previous Cole-Cole functions in the frequency domain:

$$\varepsilon^*(\omega) = \varepsilon_\infty + \sum_{i=1}^{n} \frac{\Delta\varepsilon_i}{1+(j\omega\tau_i)^{b_i}} = \varepsilon_\infty + \sum_{i=1}^{n} \Delta\varepsilon_i \Phi_i(\omega) \quad (14)$$

where $\Phi_i(\omega) = \frac{1}{1+(j\omega\tau_i)^{b_i}}$ is the relaxation function of process i. It is to note that here, the conduction term is not added to equation (14), compared to equations (2) or (10), as the fluid model already takes into account the conduction mechanisms due to charge transport (cf. j_c(x,t) in equation (12)).

We suppose here that we have n=3 relaxation modes (for instance β, β*, and α, as observed in the previous paragraph), contributing to the global dielectric response. Including equation (14) into (13) gives:

$$D(\omega) = \varepsilon_0 \varepsilon_\infty E(\omega) + \varepsilon_0 E(\omega) \sum_{i=1}^{n} \Delta\varepsilon_i \Phi_i(\omega) \quad (15)$$

Frequency to time domain conversion of the dielectric response is necessary, to obtain current transients to be compared to measurements, on the one hand, and electrical displacement, which is also accessible in experiments through space charge measurements, on the other hand.

In the time domain, the electrical displacement for the relaxation function Φ_p(t) related to the relaxation modes is given by:

$$D(t) = \varepsilon_0 \varepsilon_\infty E(t) + \varepsilon_0 \left[E(t) * \sum_{i=1}^{n} \Delta\varepsilon_i \Phi_{ip}(t) \right] \quad (16)$$

in which a convolution function between electric field and relaxation functions appears. The displacement current is derived from the electrical displacement as:

$$J_d(t) = \frac{\partial D}{\partial t} = \varepsilon_0 E(t) \left(\varepsilon_\infty \delta(t) + \sum_{i=1}^{n} \Delta\varepsilon_i \Phi_{pi}(t) \right) \quad (17)$$

Where δ(t) is the Dirac function.

In practice, each relaxation function in the time domain has been deduced from its relation with the permittivity in the frequency domain as:

$$\varepsilon'(\omega) = \varepsilon_\infty + \Delta\varepsilon \int_0^\infty \Phi_p(t) \cos(\omega t) dt \quad (18)$$

Leading to the equation, for all relaxations:

$$\sum_{i=1}^{n} \Delta\varepsilon_i \Phi_{pi}(t) = \frac{2}{\pi} \int_0^\infty g(\omega) \cos(\omega t)\, d\omega \quad (19)$$

with

$$g(\omega)=\sum_{1}^{n}\Delta\varepsilon_i\Phi_i'(\omega) \quad (20)$$

Where $\Phi_i'(\omega)$ is the real part of the relaxation function. Introducing the Cole-Cole functions in equation (20) gives:

$$g(\omega)=\sum_{1}^{n}\frac{\Delta\varepsilon_i\cos(\varphi_i)}{\left[1+2(\omega\tau_i)^{b_i}\sin\frac{\pi(1-b_i)}{2}+(\omega\tau_i)^{2b_i}\right]^{1/2}} \quad (21)$$

$\Delta\varepsilon_i, \tau_i$ and b_i are the Cole-Cole parameters previously obtained, and φ_i is also a function of the Cole-Cole parameters, and is of the form:

$$\varphi_i = arctan\left[\frac{(\omega\tau_i)^{b_i}cos\frac{\pi(1-b_i)}{2}}{1+(\omega\tau_i)^{b_i}sin\frac{\pi(1-b_i)}{2}}\right] \quad (22)$$

Changing the variable from ω to f, equation 17 becomes:

$$J_d(t) = \varepsilon_0 E(t)\left[\varepsilon_\infty\delta(t) + 4\int_0^\infty g(2\pi f)\cos(2\pi f t)\,df\right] \quad (23)$$

The above integral has been computed by discretization[26] using the real part of the inverse Fourier transform of the Matlab software, defining a frequency range [0-f_{max}] and splitting the interval into $N=2^n$ points in steps $\Delta f = f_{max}/(N-1)$. In the discretized form, equation 23 becomes:

$$J_d(t_j) = \varepsilon_0\left[\varepsilon_\infty\delta(t_j) + \Delta\Theta(t_j)\right]E(t_j) \quad (24)$$

with: $\Delta\Theta(t) = 4\int_0^\infty g(2\pi f)\cos(2\pi f t)\,df$

The relation between the j index and the time being:

$$j\Delta t = t_j \text{ with } \Delta t\Delta f = \frac{1}{2N}$$

Then

$$\Delta\Theta(t_j) = 4\frac{f_{max}}{2N-1}\sum_{1}^{N}g(2\pi k\Delta f)\cos\left[\frac{2\pi}{N}(j+1)(k-1)\right] \quad (25)$$

The input is the frequency dependence of permittivity obtained above. One of the difficulties here for the inverse Fourier transform is that only equally spaced frequency values can be used. To obtain the time response over several decades in time with a good resolution, a small step in frequency (especially for long time/low frequency) is necessary. In order to avoid using a too large number of points, the integral has been solved using different values of f_{max} (e.g. 10^{-1}, 10, 10^3… s^{-1}) and setting the number of points to 2^{20}. Then, for each frequency window, we have identified the time scale in which the precision on the $\Theta(t)$ function is the best.

The total polarization current was obtained summing up equation (23) for the different relaxation modes.

C. Comparison of experimental and simulated currents

The algorithm of the fluid model[1] is presented on Figure 6. The evolutions linked to the addition of the polarization are highlighted in red boxes. In order to validate the fluid model, which now takes into account the time-dependent permittivity, alternate polarization current (APC) measurements[11] were carried out on PEN samples. As very low electric field is applied, charge injection into the dielectric and hence conduction are minimized.

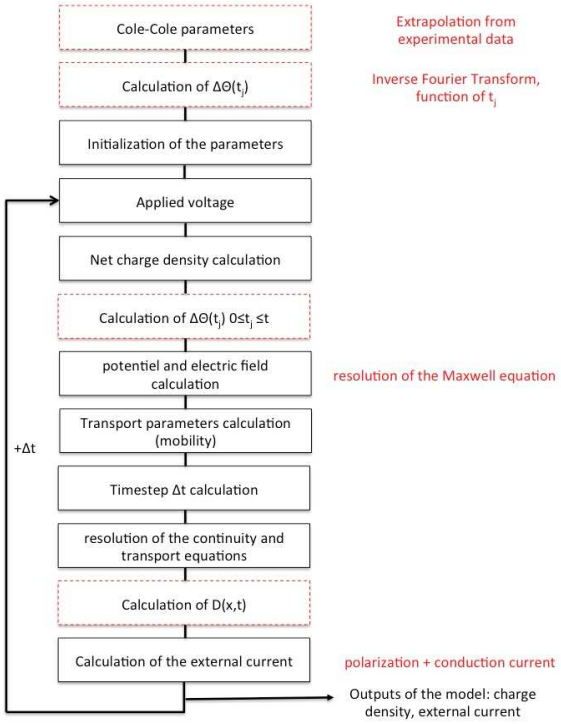

FIG. 6. Evolution of the algorithm of the fluid model of transport taking into account polarization contribution through time-dependent permittivity.

The experimental protocol is presented on Figure 7. Samples were polarized successively under low electric fields E_0 and $-E_0$ during several half-periods T/2. The polarity change between each step decreases clearly the 'memory effect' of consecutive voltage applications[27]. In our study, test films of thickness 188 or 75 µm were coated on each face with a 60mm-diameter circular gold electrode. They were polarized under low electric fields, 0.05 kV/mm during 5 half-periods of 1000s in a temperature range from room temperature to 150°C. At very low and high temperatures (-80, 130 and 150°C), a higher field was chosen (1.33 kV/mm) in order to decrease the noise level of the measured current.

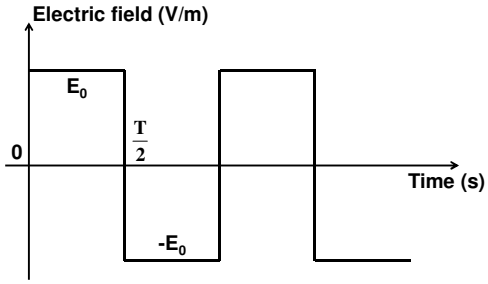

FIG. 7. Electric field protocol of APC measurements.

Figure 8 shows the normalized current densities obtained in PEN as a function of time for different temperatures. For all temperatures below 70°C, the APC current presents a linear decrease (in log-log scale) as a function of time. At temperatures above 90°C, a linear decrease is observed at short time, and then the current seems to stabilize to a constant value. If one considers that a power law dependence of the current is characteristic of polarization processes, one can conclude that, below 90°C, the measured current is dominated by orientation polarization. On the contrary when the temperature increases, polar processes are dominant at short time and conduction processes become dominant at longer time. Hence, when the temperature is high enough, APC measurements no longer reflect polarization processes only, even if the applied field is low.

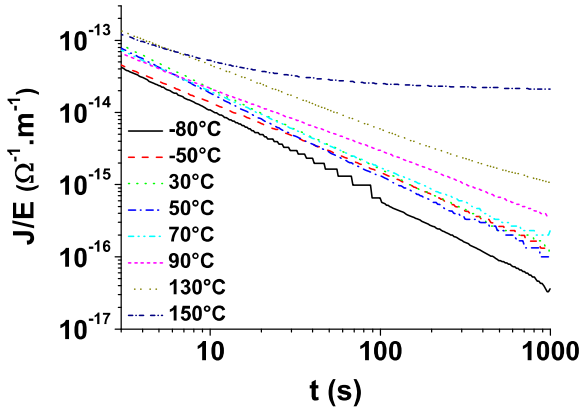

FIG. 8. APC transients for PEN as a function of time for different temperatures.

Simulations were performed for electric fields following the protocol used for APC measurements, for different temperatures. For sake of simplification, we limited our validation for temperatures ranging from -80 to 70°C, in order to remain in a temperature range where conduction processes are not dominant. The injection and transport contributions were not taken into account, in order to validate the addition of the polarization processes in the model body. At these low fields, and at relatively low temperatures, the conduction contribution should be low compared to polarization mechanisms and hence this hypothesis should hold. Hence, the external current in equation (12) is only due to the second part of the right hand side, i.e. to the variation of permittivity with time. Figure 9 shows the comparison between simulated and experimental results (current normalized to the applied field) in the time-domain and for temperatures ranging from -80°C to 70°C. It is to note that the frequencies corresponding to the time domain under study for the current measurements are in the range 10^{-3} – 1 Hz, i.e. very low frequencies.

For low temperatures (-80°C to -60°C), the comparison between experiment and simulation is consistent, as the simulated current has the same slope as the experimental one in the tested time range, and quantitative agreement is also obtained. Long time / low temperature corresponds to the low frequency region of Figure 4a. At these temperatures, and particularly at very low frequencies, only the β relaxation appears, and the maximum of the peak is well defined in the studied frequency-window.

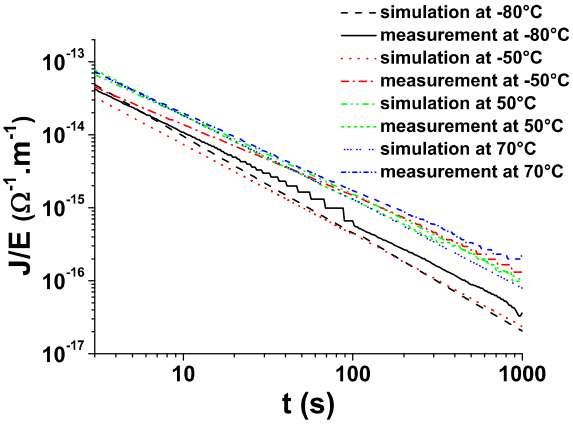

FIG. 9. Comparison of normalized currents simulated by the charge transport model and APC normalized currents at different temperatures.

For temperatures ranging from 30°C to 70°C (50 and 70°C on Figure 9), the main contribution at low frequencies comes from the β* relaxation, even if the β relaxation also contributes for a small part (see Figure 4b). For this temperature range, the simulated currents are also consistent with the experimental ones, qualitatively as well as quantitatively. One can note that at a temperature of 70°C and above, the contribution from the α-relaxation becomes non negligible at long times, i.e. low frequencies, and should be taken into account (see as an example at low frequencies in Figure 4c). However, it was not possible with our DS apparatus to properly characterize the α-relaxation peak, as the frequency range of the set-up is limited for one part, and as there is an overlapping of the α-relaxation and the conduction contributions in the dielectric response for another part. A temperature variation of the relaxation function coefficients for this relaxation could not be obtained.

For temperatures between -50°C and 30°C, the simulated results differ from the experimental ones for quite a large amount, particularly at long times. This comes from the fact that at these temperatures, and at very low frequencies, there is already a contribution from the β* relaxation (see as an example at -50°C at low frequencies on Figure 4a). The estimation of the β* contribution requires extrapolation over a very large

temperature (experimental data are obtained at around 100°C, cf. Figure 5), which actually impedes the precision as the functions for the temperature dependence of the Cole-Cole parameters are not known and might not be simple linear functions. Hence, the simulated results are quite consistent at short time (i.e. high frequency) whereas they differ from the experimental currents by one decade at longer times.

Summarizing, polarization, through a variation of the permittivity measured experimentally and fitted via Cole-Cole function, has been implemented in the body of the fluid model. The model has been validated at low fields, where polar processes remain dominant over charge transport processes. Over a large range of temperatures, the model is able to reproduce the current measured experimentally, showing that external currents measured at relatively low fields, or short time after application of the voltage for higher fields, are mainly due to polar processes. In the literature, such information has already been approached[28] by fitting the difference between the current measured under voltage and during depolarization with a power law, for fields up to 75 kV/mm at room temperature. However, no attempt was made until now to insert the variation of the permittivity in a time-dependent model to simulate current measurements.

Improvements still need to be done on the polarization description, especially for the β* contribution that would deserve a more precise characterization of the very low frequency / low temperature behavior. The α contribution could not be completely described, as the temperature range was not large enough. At high temperatures (above 90°C, where the α relaxation has a non-negligible contribution), transport processes become also non-negligible and could partially mask the α contribution.

The next step should then be to correctly parameterize the charge transport model (generation of electrons and holes, ions, trapping, detrapping coefficients, transport mechanisms) in order to reproduce the material behaviour under various thermal and electrical stresses. To do so, a large number of experimental data need to be gathered, going from space charge measurements, current measurements, electroluminescence measurements, etc.

V. CONCLUSION

Dielectric spectroscopy was used to characterize the polarization mechanisms in PEN. Three relaxation peaks were observed, β, β* and α, as polarization contributions. The first two peaks are secondary relaxations, whereas the α-peak is related to the glass transition of the material. Polarization processes were implemented in a charge transport model on the basis of experimental results provided by dielectric spectroscopy in the frequency-domain. These experimental data were fitted using Cole-Cole functions, followed by an inverse Fourier transform to get the permittivity variation in the time domain. Validation of the fluid model including polarization mechanisms was performed by comparing simulated external current and experimental current obtained under low fields in the time domain, where the response is essentially of dipolar origin. These results allow validating the data processing from the frequency-domain to the time-domain, and the implementation of the polarization processes into the fluid model. These results also demonstrate that polarization mechanisms are dominant in PEN for relatively low fields and in a large range of temperatures. More experiments need now to be performed in order to correctly parameterize the charge generation and transport processes, that are included in the fluid model, to fully describe the material behavior under higher electric fields.

ACKNOWLEDGEMENTS

The authors thank DuPont Teijin Films Co. for providing PEN samples. This work is supported by the French National Research Agency (ANR) within the ModElec project ANR-11-JS09- 009-01.

[1] S. Le Roy, G. Teyssedre, C. Laurent, G.C. Montanari and F. Palmieri, J. Phys. D.: Appl. Phys. **39**, 1427 (2006).

[2] F. Boufayed, G. Teyssèdre, C. Laurent, S. Le Roy, L.A. Dissado, P. Ségur and G.C. Montanari, J. Appl. Phys. **100**, 104105 (2006).

[3] J. Xia, Y. Zhang, F. Zheng, Z. An and Q. Lei, J. Appl. Phys. **109**, 034101 (2011).

[4] Z. Lv, X. Wang, K. Wu, X. Chen, Y. Cheng and L.A. Dissado, IEEE Trans. Dielectr. Electr. Insul. **20**, 337 (2013).

[5] S. Le Roy, P. Segur, G. Teyssedre and C. Laurent, J. Phys. D: Appl. Phys. **37**, 298 (2004).

[6] S. Le Roy, F. Baudoin, L. Boudou, C. Laurent and G. Teyssèdre, *Proc. 10th IEEE International Conference on Solid Dielectrics* (Potsdam, Germany) 703-6 (2010).

[7] S.P. Bravard and R.H. Boyd, Macromolecules **36**, 741 (2003).

[8] E. Logakis, L. Petersson and J. Viertel, *Proc. 11th IEEE International Conference on Solid Dielectrics* (Bologna, Italy) 948-51 (2013).

[9] M-Q. Hoang, L. Boudou, S. Le Roy and G. Teyssedre, J. Phys. D: Appl. Phys. **47**, 455306 (2014).

[10] J.C. Canãdas, J.A. Diego, M. Mudarra, J. Belana, R. Díaz-Calleja, M.J. Sanchis and C. Jaimés, Polymer **40**, 1181 (1999).

[11] C. Escribe-Filippini, R. Tobazéon and J.C. Filippini, *Proc. 7th IEEE International Conference on Solid Dielectrics* (Eindhoven, Netherlands) 315-8 (2001).

[12] R. Eveson, W.A. MacDonald, D. MacKerron, A. Hodgson, R. Adam, K. Rakos, K. Rollins, R. Rustin, M.K. Looney, J. Stewart, M. Asai and K. Hashimoto, SID Int. Symp. Dig. Tech. Papers **39**, 1431 (2008).

[13] B. Schartel and J.H. Wendorf, Polymer **36**, 899 (1995).

[14] J.C. Coburn and R.H. Boyd, Macromolecules **19**, 2238 (1986).

[15] C. Hakme, I. Stevenson, L. David, G. Boiteux, G. Seytre and A. Schönhals, J. Non-cryst. Solids **351**, 2742 (2005).

[16] H. Dortliz and H.G. Zachmann, J. Macromol. Sci. B: Phys. **36**, 205 (1997).

[17] J.J. Martinez-Vega, N. Zouzou, L. Boudou and J. Guastavino, IEEE Trans. Dielectr. Electr. Insul. **8**, 776 (2001).

[18] K.H. Illers and H. Breuer, J. Colloid Sci. **18**, 1 (1963).

[19] J. Belana, M. Mudarra, J. Calaf, J.C. Canãdas and E. Menéndez, IEEE Trans. Electr. Insul. **28**, 287 (1993).

[20] J.P. Bellomo and T. Lebey, J. Phys. D.: Appl. Phys. **29**, 2052 (1996).

[21] S. Havriliak and S. Negami, Polymer **8**, 161 (1967).

[22] K.S. Cole and R.H. Cole, J. Chem. Phys. **9**, 341 (1941).

[23] A. Nogales, Z. Denchev, I. Sics and T.A. Ezquerra, Macromolecules **33**, 9367 (2000).

[24] L. Hardy, I. Stevenson, A. Fritz, G. Boiteux, G. Seytre and A. Schönhals, Polymer **44**, 4311 (2003).

[25] C.J.F. Böttcher and P. Bordewijk, *Theory of Electric Polarization, Vol. II: Dielectrics in time-dependent fields*, Verlag Elsevier Ed., Amsterdam, 1978.

[26] M. Ambid, "Evaluation de nanocomposites polypropylène/silicate pour l'isolation électrique : Etude des phénomènes de polarisation, de conduction et des propriétés optiques", Ph D Thesis, Paul Sabatier University – Toulouse III, 2007.

[27] V. Adamec and J.H. Calderwood, J. Phys. D: Appl. Phys. **14**, 1487 (1981).

[28] J.L. Augé, G. Teyssedre, C. Laurent, T. Ditchi and S. Holé, J. Phys. D: Appl. Phys. **33**, 3129 (2000).